



Variability of precipitation extremes over the Yangtze River Delta, eastern China, during 1960–2016

Jia Yuan¹ · Youpeng Xu¹ · Lei Wu¹ · Jie Wang¹ · Yuefeng Wang¹ · Yu Xu¹ · Xiaoying Dai¹

Received: 11 March 2018 / Accepted: 27 February 2019 / Published online: 12 March 2019
© Springer-Verlag GmbH Austria, part of Springer Nature 2019

Abstract

Understanding the changing characteristics and related mechanisms behind precipitation extremes is crucial for developing adaptive measures of water resource management as well as flood risk management. Based on daily precipitation measurement taken at 57 meteorological stations from 1960 to 2016, the variability of precipitation extremes over the Yangtze River Delta (YRD) is analyzed utilizing a Mann-Kendall trend test as well as a Hurst exponent analysis. Moreover, the climatic teleconnection that occurs from large-scale atmospheric circulation and such precipitation extremes is also investigated with the help of a wavelet coherence analysis. Results indicate that most extreme precipitation indices predominantly exhibit significant positive trends, indicating a wetting trend in the YRD over the past 61 years. Meanwhile, the contribution of precipitation of very wet days to annual total wet-day precipitation increased significantly. Furthermore, the increasing trend of precipitation extremes in the YRD is found to be attributable to the frequency and intensity, rather than to the duration of extreme precipitation events. The patterns of variation in these precipitation extremes reveal dramatic spatial heterogeneity, with extreme events concentrated primarily along the coastal plains. Overall, the YRD will likely face more severe flood risks in the foreseeable future. This is especially the case for the southern and central-western regions of the YRD. In contrast, the northern region of the YRD is forecast to become drier over time. The increasing trends in precipitation extremes for the YRD observed in this study are found to be linked closely with the positive anomalies of the El Niño-Southern Oscillation as well as the negative anomalies of the East Asian summer monsoon.

1 Introduction

Precipitation is not only a chief element in the Earth's hydrological cycle, but is also a crucial regulating factor in atmospheric circulation (Limsakul and Singhruck 2016; Tapiador et al. 2017). Variabilities in precipitation generally, and extreme precipitation specifically, have already placed severe pressure on water safety, societal infrastructure, and social economy, provoking large-scale outbreaks of waterborne disease as well as an increasing body count from related natural disasters worldwide (Curriero et al. 2001; Hossain et al. 2010; Shimizu et al. 2017). Quantitatively investigating the changes in extreme weather and climate events of the past (e.g., floods, flash-floods, rainstorm, droughts, and heat waves) is a critical prerequisite for the understanding of the response that the

hydrological cycle as well as water resource variability will have to change in climate at the local, regional, and even global scale (IPCC 2013; Zhang et al. 2014; Xiao et al. 2017). Consequently, there is an urgent need for adequate monitoring and prediction when it comes to the variation of frequency, intensity, and duration in precipitation extremes. This is essential for developing the appropriate tools, techniques, and infrastructure in hydraulic engineering that is needed to reduce the adverse impacts associated with extreme precipitation events. Moreover, the findings of studied therein offer excellent opportunities for exploring the possible physical mechanisms behind climate change, contributing to great understanding in the research community.

The extreme meteorological and hydrological events seen over the last few decades, commonly attributed to climate change, have generated extensive concern among the world's government, scientific community, and the general public. Generally speaking, both a widespread and significant increasing trend in precipitation extremes are identified in more land areas around the world (Alexander et al. 2006; Donat et al. 2013; Asadieh and Krakauer 2015). Nevertheless, the

✉ Youpeng Xu
xypnju@163.com

¹ School of Geographic and Oceanographic Sciences, Nanjing University, Nanjing 210023, China

observed patterns of change therein are oftentimes complex and spatially heterogeneous when scaled regionally. Simply put, different regions will exhibit contradictory trends. For example, negative trends in extreme precipitation events have been discovered in Northeast China, Northern China, the Yellow River basin, as well as the northwest and southeast regions of the Loess Plateau. Contrary to these findings, positive trends in extreme precipitation events have been observed in south-eastern Chinese coast, Northwest China, the Tibetan Plateau, as well as the middle and lower reaches of the Yangtze River (Fu et al. 2013; Wan et al. 2014; Gao and Wang 2017). In the research of Duan et al. (2015), it was found that despite the fact that the annual and seasonal precipitation observations taken throughout Japan from 1901 to 2012 exhibited a downward trend, most of sample's indices for precipitation extremes exhibited a contradicting but synchronized trend toward increase. Additionally, observational evidence paired with multi-model simulations has indicated that precipitation extremes are likely to continue to intensify in many regions around the world in the context of global warming well into the future (Kao and Ganguly 2011; IPCC 2013; Qin and Xie 2016). It has been found that the world's dry regions are similarly projected to suffer from an increased risk of flooding under such conditions (Donat et al. 2016).

In addition to global warming, large-scale atmospheric circulation also has a dramatic impact on precipitation extremes (Liu et al. 2017). The El Niño-Southern Oscillation (ENSO) affects changes in the atmospheric-oceanic system of the tropical regions of the Pacific Ocean, forcing significant influence on changes in climate worldwide; however, the effects of the ENSO are asymmetric (Ward et al. 2014; Sun et al. 2015; Tedeschi et al. 2015). In fact, the research of Grimm and Tedeschi (2009) revealed that the ENSO brings about more spatial coherence changes in frequency of extreme events when compared with the changes in the intensity of extreme events, and that changes in daily extreme precipitation in South America are more sensitive to the influence of the ENSO than they are to the region's changes in total monthly precipitation. Shimizu et al. (2017) found that most extreme dry events in the Amazon Basin and Northeast Brazil will occur during El Niño periods, while extreme precipitation events are more common during La Niña period or neutral years.

Depending on the different peaks in sea surface temperature that occur in a given year, extreme meteorological events during El Niño can be assorted into two different categories, namely the Eastern-Pacific El Niño and the Central-Pacific El Niño (Kug et al. 2009). These two types of El Niño have a correspondingly different influence on the climate of the Asia-Pacific region. Specifically, an Eastern-Pacific El Niño can lead to heavy rainfall in northern Peru whereas a Central-Pacific El Niño will be associated with decreased rainfall over the upstream regions along the Pacific Slope (Bourrel et al.

2015; Rau et al. 2017). Additionally, Curtis (2008) found that precipitation intensity in Florida specifically, and the Southeast coast of the USA generally, will be enhanced during the warm phase of the Atlantic Multidecadal Oscillation while extreme precipitation will correspondingly be decreased in the Northwest Mexico.

As one of the most rapidly urbanized, densely populated metropolitan agglomerations in the world, the Yangtze River Delta (YRD) has played and continues to play a crucial role in the economic development in China as a whole. Simultaneously, the YRD is also an area that is remarkably susceptible to changes in climate due to its characteristically large variation in precipitation levels. Past research has demonstrated that flood disaster risk in the central and southern areas of the YRD has increased dramatically over the past half century, and that the intensity of precipitation therein has likewise intensified considerably (Han et al. 2015; Wang et al. 2016). Unfortunately, it must be noted that this past researcher focused primarily on spatiotemporal variation in extreme precipitation. The questions of how extremes in precipitation across the YRD can be affected by large-scale atmospheric circulation remain unaddressed.

This study investigates the changes in observed across the YRD from 1960 to 2016 in order to explore the relationship between variability in regional precipitation extremes and large-scale atmospheric circulation. The remainder of this paper is organized as follows. The study's datasets and methodology are introduced in Sect. 2. Descriptive and inferential results of variability are described in Sect. 3. The potential relationship between regional precipitation extremes and large-scale atmospheric circulation are discussed in Sect. 4. Conclusions are presented last, in Sect. 5. The study's results are expected to provide useful information for developing adaptive measures in water resource management as well as flood risk prevention and control.

2 Data and methodology

2.1 Study area

What constitutes the total area of the YRD will vary from profession to profession. For this study, the term YRD specifically refers to the economic definition of the area, rather than the area commonly denoted in geomorphology. To be exact, the YRD (27°01' N~35°20' N; 114°54' E~123°08' E) is located on the lower reaches of the Yangtze River in Eastern China and includes three provinces and one municipality, with a total area approximately of 344,300 km². Jiangsu Province (JSP), Zhejiang Province (ZJP), and Anhui Province (AHP) are distributed in the north, south, and west, respectively. The densely populated Shanghai municipality is centrally located along the region's coastline (Fig. 1). The region is characterized by high

elevation in the southern as well as western areas and characterized by low elevation in its central, eastern, and northern areas. Covered by the East Asian monsoon climate, annual precipitation in the study area exhibited a high degree of spatial heterogeneity that is consistent over time, with a predictable and abundant level of precipitation during the region’s flood season (specifically, from May to September). Moreover, the region’s coastal areas are particularly vulnerable to typhoons and tides owing to the area’s flat and low topography.

Covering approximately 3.59% of the total area of China, the YRD supports 16.1% of the Chinese population regardless, contributing to 23.82% of the nation’s gross domestic product. The rate of urbanization (that is, the urbanization of population) for the YRD was nearly 68.65% in 2016, exceeding the national average by 11.3% (National Bureau of statistics of the People’s Republic of China 2017).

2.2 Data

2.2.1 Data sources

The daily precipitation observation data utilized for this study were acquired from the National Meteorological Information

Center of the China Meteorological Administration (<http://data.cma.cn>). After carefully considering various criteria for continuity, the largest time interval over the largest geographic coverage was found in 59 representative meteorological stations, all located within the YRD (Fig. 1). With the sole exception for the data taken from the “Dinghai” station (specifically spanning from 1963 to 2016), the data taken from all other stations span from 1960 to 2016. Note that the percentage of missing data herein accounted for less than 1% of the study’s total data. Specifically, the procedure for substituting any missing data was as follows. If any data were missing for 1 or 2 days, they were replaced by the average values of the days directly preceding and following each block of missing data. Otherwise, the missing data were replaced by the averages for the same days of all other years in the study’s sample pool (Zhang et al. 2011a).

In addition, in order to evaluate the relationship between large-scale atmospheric circulation and variation in precipitation extremes, this study adopted the Multivariate ENSO index (MEI) as well as the Pacific Decadal Oscillation (PDO) sea surface temperature dataset, both provided by the National Oceanic and Atmospheric Administration’s Earth System Research Laboratory (<http://www.esrl.noaa.gov/psd/ens-o/mei/index.html>). The East Asian summer monsoon index

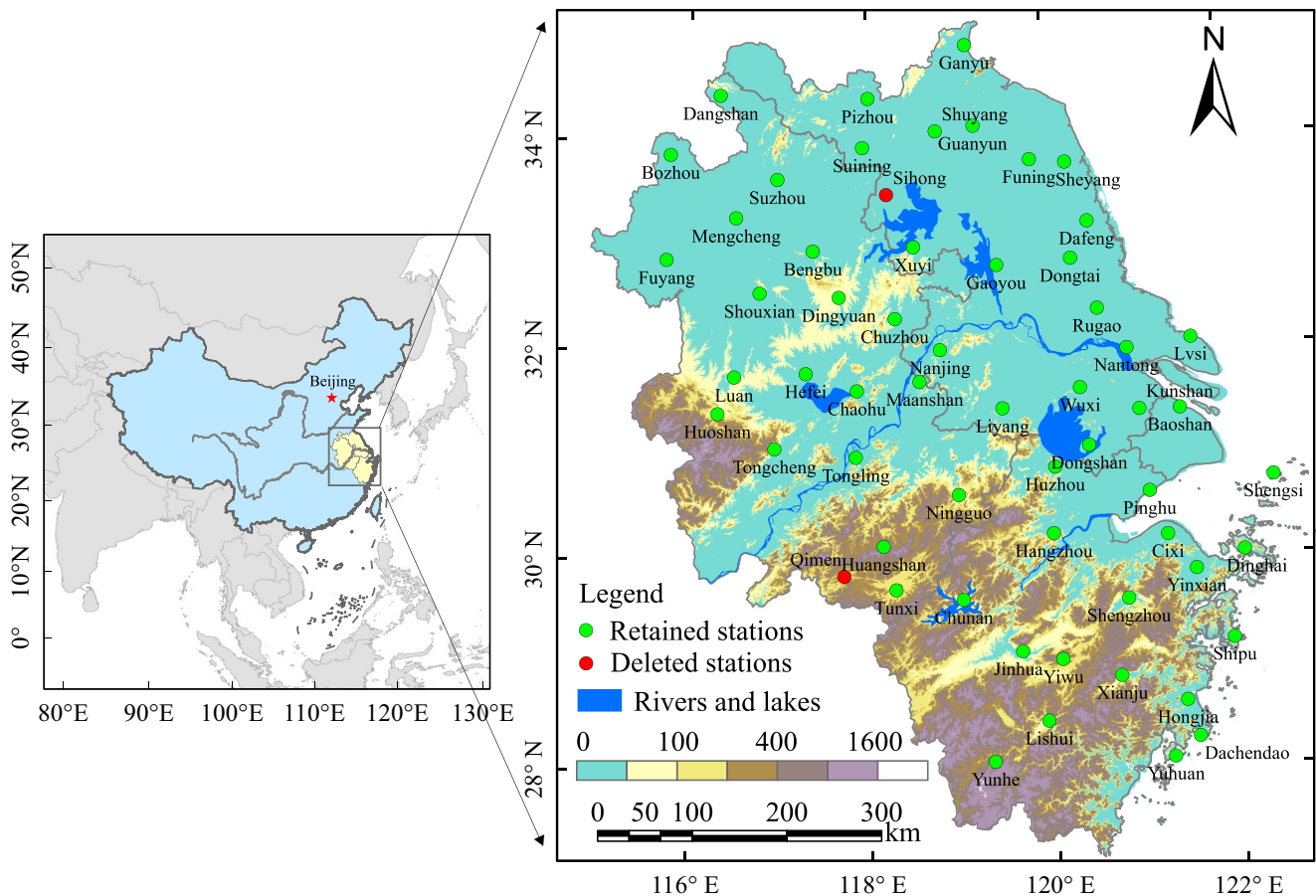


Fig. 1 The geographical location and distribution of the meteorological stations in the YRD used in this study. The red circle denotes the stations whose measurements were invalid, and thus excluded for consideration. The green circle denotes the stations whose measurements were included

(EASMI) (<http://ljp.gcess.cn/dct/page/1>) as defined by Li and Zeng (2002, 2005) was also adopted for this study to these ends.

2.2.2 Quality control and homogeneity testing for the study's data

Quality control for the data in weather and climate studies is crucial. Proper parsing can detect errors in meteorological data, such as negative values for daily precipitation or values that are greater than the maximum possible (Llabrés-Brustenga et al. 2019). For this study, the RClimDex software (<http://etccdi.pacificclimate.org/software.shtml>) developed by the Climate Research Branch of the Meteorological Service of Canada was utilized to conduct quality control checks for the study's sample data. Any identified potential outliers were manually checked and then either, validated, adjusted, or deleted.

Likewise, utilizing homogeneous and long-term climate records is instrumental in conducting robust analyses regarding climate events. Unfortunately, due to a plethora of logistical concerns (e.g., change in station location, instrument or observational practice, and environment), the long-term data series for climatic measures will invariably exhibit some shortcoming in homogeneous or continuity that make observational data a somewhat inaccurate reflection of the reality of a locale's climate situation (Peterson and Manton 2008; Zhang et al. 2011b). To check for such shortcomings, the RHtests_dlyPrp software package (<http://etccdi.pacificclimate.org/software.shtml>) was employed to assess homogeneity in the study's sample data. After examining the observational data for all 59 stations, the precipitation series for the "Qimen" and "Sihong" stations (highlighted with a red circle in Fig. 1) were found to have unacceptable change points in 1996 and 1980, respectively. Thus, these two stations were excluded entirely in the study's analyses, and the remaining 57 homogeneous stations (highlighted with a green circle in Fig. 1) exhibited no such problems and were thus utilized in full.

2.3 Methods

2.3.1 Extreme precipitation indices

A specific set of indices are advocated by the Expert Team on Climate Change Detection and Indices (ETCCDI) in their ability to effectively describe and assess variability in extreme weather events in terms of intensity, frequency, and duration (WMO 2009). These indices can provide clear definitions, as well as a uniform calculation standard, for extreme climate events. Furthermore, the ETCCDI has also developed a corresponding software packages (notably including RClimDex and FClimDex) to calculate these indices. Thus, by using these uniform indices and the corresponding software suite suggested by the ETCCDI, analyses that are carried out in

any part of the world can fit together seamlessly for pragmatic comparison (Alexander et al. 2006; Peterson and Manton 2008). It must be noted that these tools have helped to make great contribution in the technical capacity as well as theoretical development for researcher in the field of climate change conducting their studies on the global scale. As represented in Table 1, this study adopted nine of these indices in order to analyze the variability of precipitation extremes over the YRD. Detailed descriptions for each of these indices can be found in relevant reports or papers (Klein Tank et al. 2009; Zhang et al. 2011b). Specifically, the software program RClimDex was used to calculate the indices for this study.

2.3.2 Trend analysis

A frequently used method for detecting trend in variation for hydrometeorological data series is the nonparametric Mann-Kendall test (Kendall 1955; Dietz and Killeen 1981; Hirsch et al. 1982). In fact, this test is specifically recommended by the World Meteorological Organization. When compared with other meteorological methodologies, the Mann-Kendall test does not require samples to comply with certain distributions or variance homogeneity and is resistant to the effects of outliers as well (Gan 1998; Duhan and Pandey 2013). A positive value for the statistical eigenvalue Z_S will denote an increasing trend, while a negative value will denote a decreasing trend (Xu et al. 2018). For this study, a trend was considered statistically significant so long as it was found to be statistically significant at 0.05 level. In addition, the least squares method was adopted for this study as well, in order to estimate the rate of the change for the statistical trends found on the decade scale.

2.3.3 Hurst exponent analysis

The Hurst exponent, as estimated via a classical rescaled range analysis, is a practical method for detecting the long-term processes that occur in time series (Sánchez Granero et al. 2008). It must be noted that this method does in fact have a few assumptions required of the object of study, but that the method has become widely adopted and has been shown to be a robust statistical method regardless. To clarify, the central calculation processes for the Hurst exponent are as follows (Sánchez Granero et al. 2008):

1. To define the time series $\{\xi(t)\}$ ($t = 1, 2, \dots, n$) and divide the time series into τ sub series $x(t)$.
2. To define the arithmetic mean sequence of the time series, such that:

$$\xi_\tau = \frac{1}{\tau} \sum_{t=1}^{\tau} x(t) \quad \tau = 1, 2, \dots, n \quad (1)$$

Table 1 The definitions for the nine precipitation indices used in this study

Index	Descriptive name	Definition	Units
PRCPTOT	Annual total wet-day precipitation	Annual total PRCP in wet days (RR >= 1 mm)	mm
R95p	Very wet days	Annual total PRCP when RR > 95th percentile	mm
R10	Number of heavy precipitation days	Annual count of days when PRCP ≥ 10 mm	Days
R20	Number of very heavy precipitation days	Annual count of days when PRCP ≥ 20 mm	Days
RX1day	Max 1-day precipitation amount	Monthly maximum 1-day precipitation	mm
Rx5day	Max 5-day precipitation amount	Monthly maximum consecutive 5-day precipitation	mm
CDD	Consecutive dry days	Maximum number of consecutive days with RR < 1 mm	Days
CWD	Consecutive wet days	Maximum number of consecutive days with RR ≥ 1 mm	Days
SDII	Simple daily intensity index	Annual total precipitation divided by the number of wet days (defined as PRCP ≥ 1 .0 mm) in the year	mm day ⁻¹

RR denotes daily rainfall; a wet day is defined specifically as when RR ≥ 1 mm. A dry day is defined specifically as when RR < 1 mm

3. To calculate cumulative deviation, such that:

$$X(t, \tau) = \sum_{u=1}^t (\xi(u) - \langle \xi \rangle_\tau) \quad 1 \leq t \leq \tau \tag{2}$$

4. To calculate the range sequence, such that:

$$R(\tau) = \max_{1 \leq t \leq \tau} X(t, \tau) - \min_{1 \leq t \leq \tau} X(t, \tau) \quad \tau = 1, 2, \dots, n \tag{3}$$

5. To calculate the sequence of standard deviation, such that:

$$S(\tau) = \left[\frac{1}{\tau} \sum_{t=1}^{\tau} (\xi(t) - \langle \xi \rangle_\tau)^2 \right]^{\frac{1}{2}} \quad \tau = 1, 2, \dots, n \tag{4}$$

6. To calculate the Hurst exponent, such that:

$$\frac{R(\tau)}{S(\tau)} = (c\tau)^H \tag{5}$$

Specifically, the variable *H* denotes the Hurst exponent itself, which can be acquired by using least-squares fitting within a double logarithmic coordinate system. The value of *H* will lie between 0 and 1, and it can be split into three cases (Hurst 1951; Mandelbrot and Wallis 1969). First, a value of *H* = 0.5 indicates that the time series is simply a random walk, without sustainability. This means that the trend for future change for the time series will be unrelated to any historical trends. Second, a value of 0.5 < *H* < 1 will imply sustainability in the series, indicating how the trend of future change for the time series will be similar to historical trends. A greater value will indicate greater sustainability therein. Third, a value of 0

< *H* < 0.5 indicates a trend of anti-sustainability for the time series into the future. Here, the lower the value, the greater the anti-sustainability.

2.3.4 The wavelet coherence analysis

The continuous wavelet transform has been widely utilized in research to analyze the dominant modes of variability in hydrometeorological time series (Torrence and Compo 1998; Wang et al. 2016). However, a notable limitation to this method must be noted in that it cannot reflect correlations between two time series. A useful technique, commonly referred to as wavelet coherence, can fortunately resolve this limitation in its capacity to reveal the intensity of covariance as well as coupled oscillations in various domains of both time and frequency between two time series (Torrence and Compo 1998; Zhang et al. 2007). Wavelet coherence can work to treat as a localized correlation coefficient in time and frequency space. Additionally, Monte Carlo models were employed in this study to test significance levels against red noise using autoregressive processes (Grinsted et al. 2004; Yin et al. 2016). Given the advantages presented in the utilization of a wavelet coherence methodology, the method was adopted for this study specifically in order to illustrate the cross-correlation that occurs between extreme precipitation and large-scale atmospheric circulation. The MATLAB coding used in this study was acquired from <http://www.glaciology.net/wavelet-coherence>.

3 Results

3.1 General situation of precipitation

A brief introduction to the general situation regarding precipitation in the study’s area will be helpful for

better understanding variability in precipitation extremes. A contour map of the mean annual precipitation (MAP) in the YRD, as observed from 1960 to 2016, is presented in Fig. 2. Generally speaking, the MAP presents an increasing trend in precipitation from north to south, characterized by a high level of spatial variability. It is found that the higher and lower values in the MAP were generally distributed along its south-western and north-western areas, with the highest and lowest values recorded in 2016 and 1978, respectively.

Figure 3 illustrates the patterns of change in precipitation that occurred, at both monthly and decadal intervals, from 1960 to 2016. In Fig. 3a specifically, the YRD received the highest levels of precipitation from June to July and lowest levels of precipitation from December to January. Moreover, significant increasing trend in precipitation is found to occur from January to February, while an insignificant decreasing trend was detected from April to May and September to October. These findings indicate that the region's spring and autumn periods have become increasingly drier over the sample period, whereas its winters have become increasingly wetter. Additionally, it can be seen in Fig. 3b that the volume of precipitation exhibited an upward trend on the decadal scale. Herein, the highest and lowest values were recorded in the 2010s and 1960s, respectively.

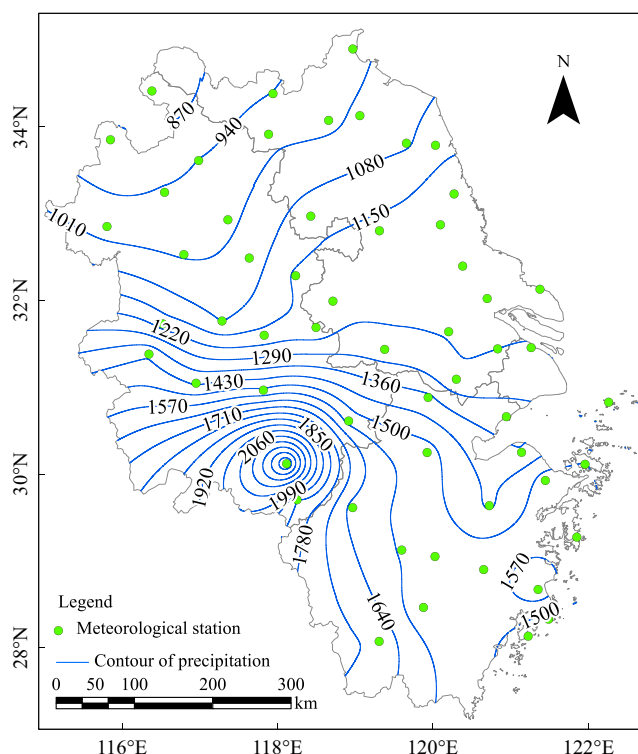


Fig. 2 The spatial distribution pattern for annual total precipitation over the YRD from 1960 to 2016

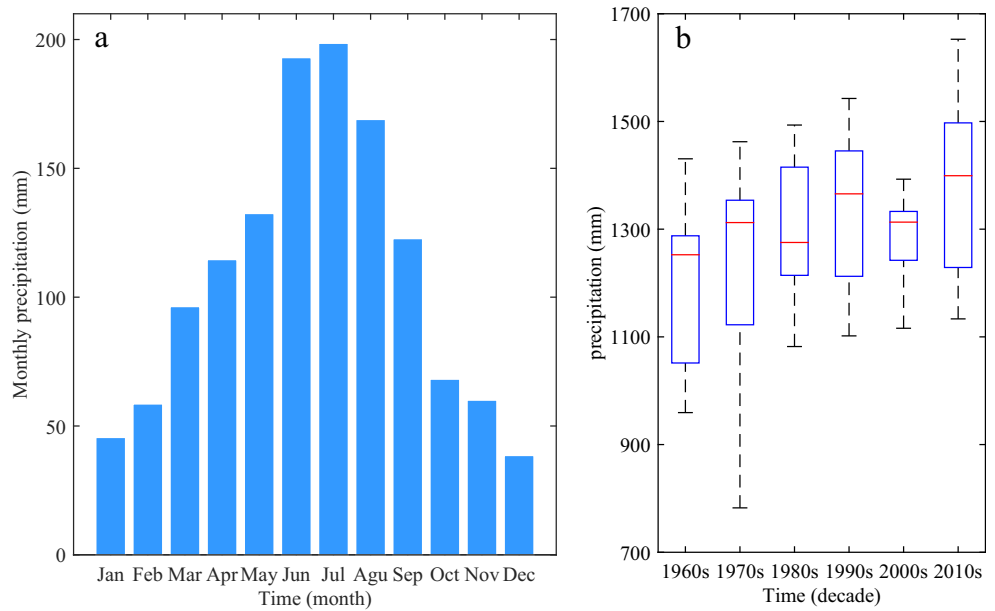
3.2 Variation in precipitation extremes over time

The regionally averaged annual variation in the study's precipitation indices covering the YRD from 1960 to 2016 are depicted in Fig. 4. It can be seen that, with the exception of consecutive wet days (CWD) and consecutive dry days (CDD) indices, positive trends dominate all of the study's other. As seen in Fig. 4a, the mean annual total wet-day precipitation (PRCPTOT) reveals a significant increasing trend with a linear tendency toward a 26.9 mm increase per decade. As seen in Fig. 4b, the precipitation in very wet day (R95p) similarly exhibited a significant positive trend, increasing at 18.3 mm per decade. For all observation stations, the largest recorded value of R95p was found at the Huangshan station, with 1810.4 mm of rainfall measured in 2016. Furthermore, it can be seen in Fig. 4c, d that a subtle variability is present over all max 1-day precipitation amount (Rx1day) and max 1-day precipitation amount (Rx5day) measurement, though this merely represents an insignificant uptrend, at 1.8 mm and 3.3 mm per decade, respectively. At the station scale, the highest values for Rx1day and Rx5day were observed at the Baoshan station in 1987 and Tongcheng station in 1969, at 394.5 mm and 705.8 mm, respectively. On the contrary, it can be seen in Fig. 4e, f that the mean annual number of heavy precipitation days (R10 mm) and number of very heavy precipitation days (R20 mm) all showed significant increasing trends and that a rapid rise is also present in both during the sample period's final decade. In considering each individual station, the highest values for R10 mm and R20 mm were found to all occur at the Huangshan station, located in the south-western area of the YRD, in 1973.

An exception from all the study's other indices can be found in Fig. 4g, h, in that an insignificant falling trend is prevalent in the CWD and CDD indices. Specifically, it was found that the mean annual CWD and CDD were 7.91 days and 33.34 days, respectively. The highest values for CWD and CDD were found in 1992 and 1974, being 10.21 days and 69 days, respectively. The variation in CWD exhibited an uptrend in fluctuation from 1960 to 1990, with a noticeably rapid decline thereafter. The greatest values for CWD and CDD were measured at the Ningguo station and Mengcheng stations, in 1977 and 1974, at 24 days and 113 days, respectively. Additionally, annual simple daily intensity index (SDII) was found to exhibit a significant upward trend, with a tendency for 2.4 mm day⁻¹ per decade (Fig. 4i). Notably, it was also found that SDII was significantly larger over the last few decades than it was earlier periods of measurement.

Furthermore, it was found that contribution of R95p to PRCPTOT was between 16.12 and 37.11%. These ratios rose dramatically by the decade, namely from 22.8% in the 1960s and then upward to 35.23% in the 2010s, with a tendency of 2.36% growth per decade. Considering how the frequency and intensity of the observed precipitation extremes was an

Fig. 3 The patterns of precipitation across the YRD from 1960 to 2016 at the monthly (a) and decadal scale (b). The top and bottom sections of the boxes are the first and third quartiles, while the bands inside said boxes denote the second quartiles (i.e., medians)



increase while duration correspondingly decreased, the increasing trend of precipitation extremes in the YRD can be

attributed overall to frequency and intensity, rather than to duration.

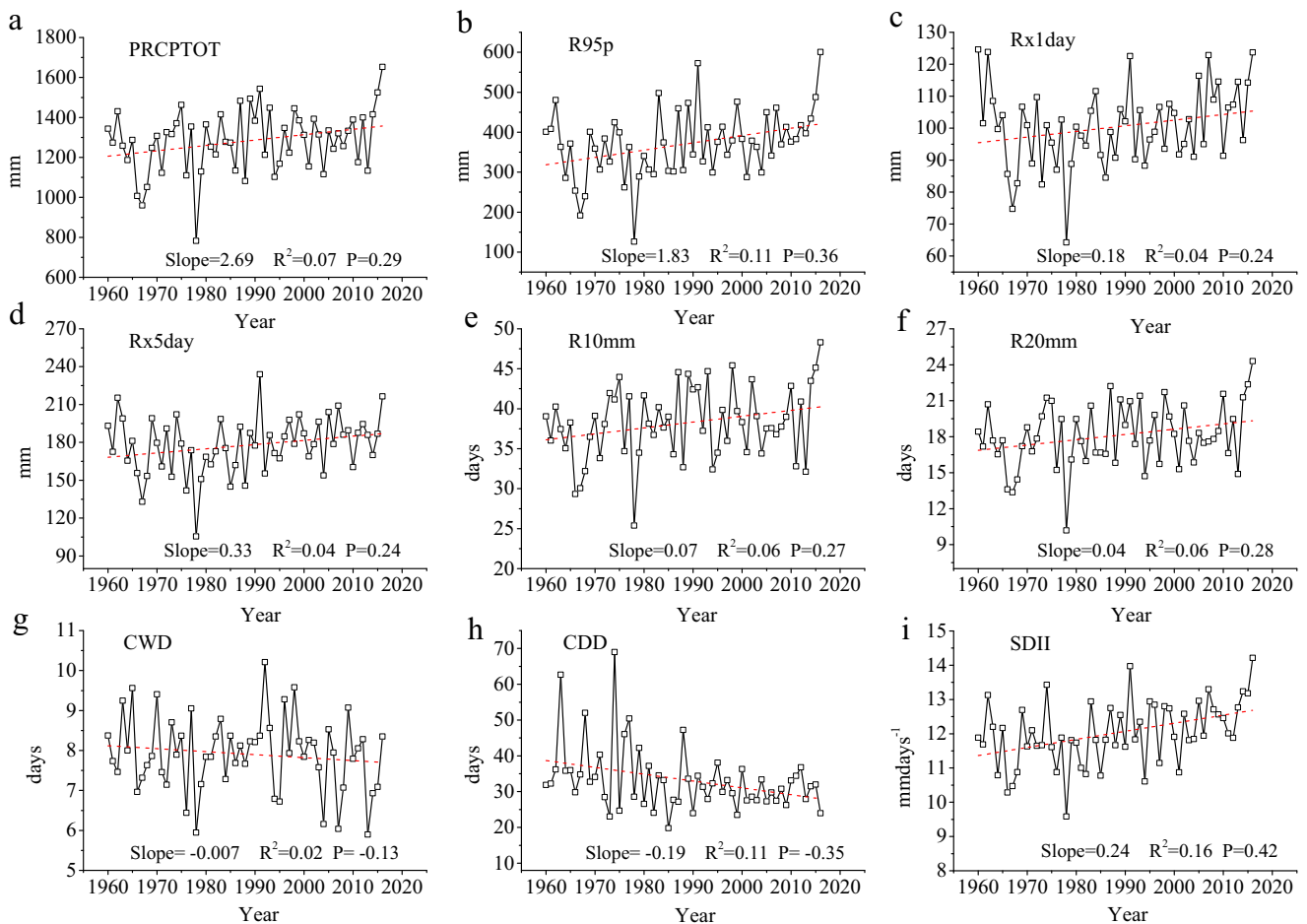


Fig. 4 The regionally averaged annual series for the study’s extreme precipitation indices in the YRD from 1960 to 2016. The red dashed lines denote the linear trend

3.3 Spatial distribution of precipitation extremes

The spatial distribution patterns as well as the variability tendencies for the study's precipitation indices covering the YRD from 1960 through 2016 are presented in Fig. 5. The categories and degree of change trends (i.e., significant increase, insignificant increase and decrease, and significant decrease) are presented in Fig. 6. As seen in Fig. 5a, b, PRCPTOT and R95p exhibited similar trends in both variation as well as spatial distribution. For PRCPTOT, about 82% of all sample measurement stations revealed a positive trend. Furthermore, significant uptrends were reported in 26.3% of stations (Fig. 6). By contrast, the stations in the northern areas of AHP and JSP displayed slightly downward. However, it must be noted that only one station's measurements were found to be significant in this last case of downward trend. With respect to

R95p, the proportion of stations with positive trends was found to be 84%. It was found that the stations that exhibited negative trends were concentrated primarily in the region's northern and western areas (Fig. 6b). Of all measuring stations, 12.2% exhibited significant positive trends. No stations indicated a negative trend that was significant.

As illustrated in Fig. 6, 72% and 75% of the study's stations exhibited a rising trend in Rx1day and Rx5day, respectively. Of them, 12.2% and 5.3% were found to be significant, exhibiting a scattered and sporadic distribution. The measuring stations that presented positive trends in Rx1day and Rx5day were principally located in the western, south-western, and south-eastern areas of the YRD. From Fig. 5c, d, it can be seen that the magnitude of increase in the western areas is considerably larger than that of south-eastern area. On the other hand, the negative trends for Rx1day and Rx5day were

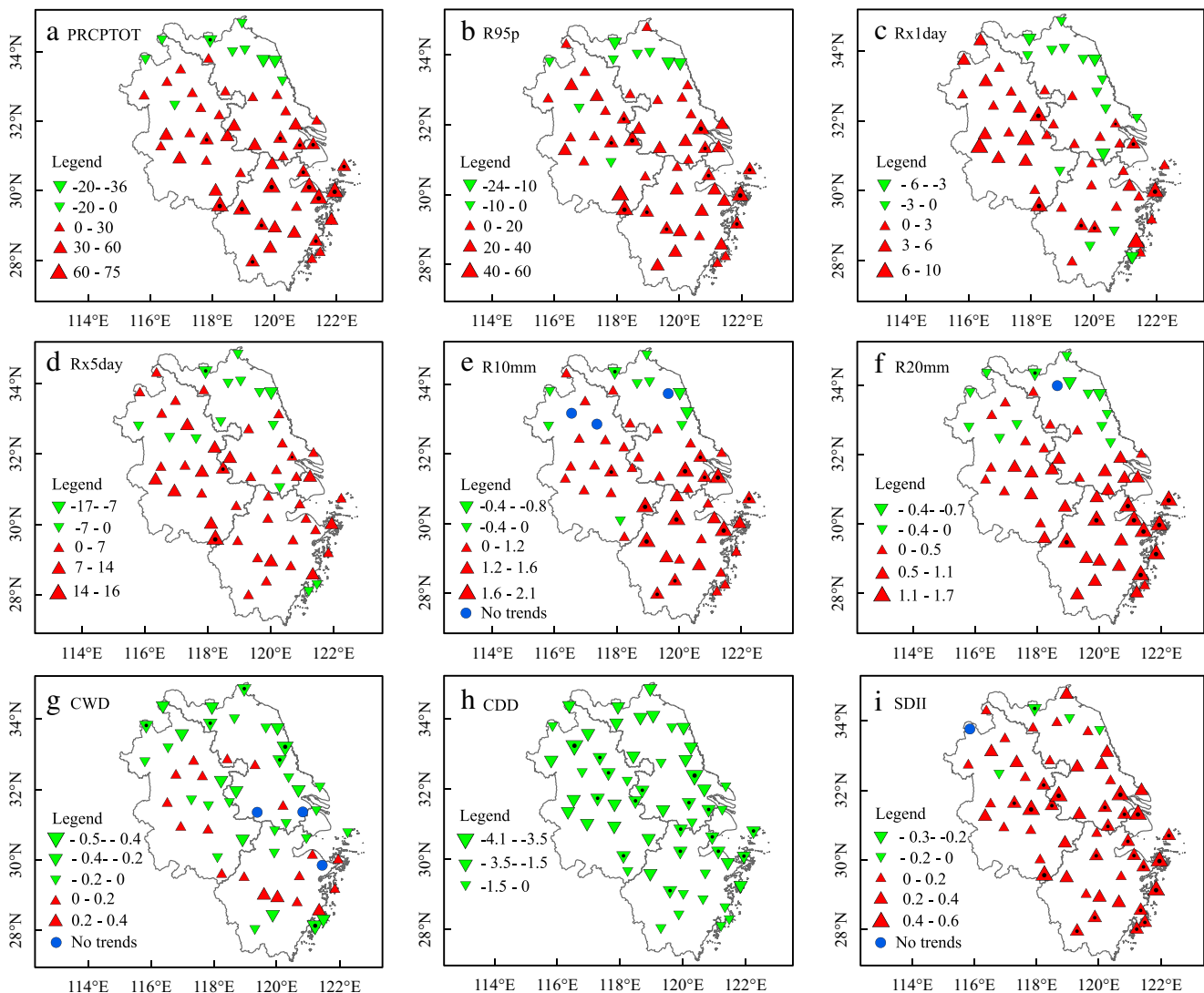
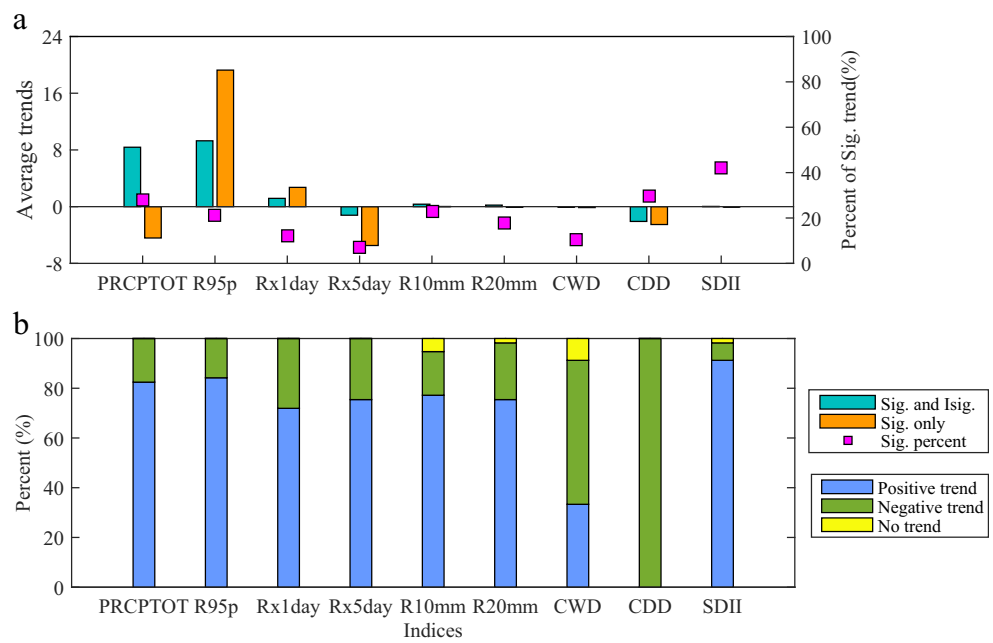


Fig. 5 The trends in the study's extreme precipitation indices, per period, from 1960 to 2016 for **a** PRCPTOT, **b** R95p, **c** Rx1day, **d** Rx5day, **e** R10 mm, **f** R20 mm, **g** CWD, **h** CDD, and **i** SDII. The triangles are

scaled by the magnitude of the trend. Red denotes increasing trends, blue denotes no trend, while green denotes decreasing trends. The trends that are significant at 0.05 level are highlighted with black dots

Fig. 6 The regionally averaged trends found in the study's extreme precipitation indices (a). The percent of different types of change in the YRD from 1960 to 2016 (b)



distributed primarily around the north-eastern area of the study region. Notably, this last finding is in accordance with the spatial distribution of the trends found for PRCPTOT. For R10 mm, 21.05% of stations exhibited significant rising trends (Fig. 6). Moving on, it can be seen from Fig. 5e that the regions that exhibited the largest rates of increase were predominantly located in the central and south-western areas of the YRD. The stations that observed decreases were located primarily around the north-eastern area. The measurements for one of these latter stations were found to be significant. In addition, approximately 73% of all stations exhibited an increasing trend for R20 mm. These stations were principally situated over the southern area of the study region. From Fig. 5f, it can be seen that the magnitude of this rising trend generally grows as one moves from west to east. Conversely, falling trends were generally observed in the YRD's northern areas.

However, it must be noted that the spatial distribution for CWD was found to be rather complex. Approximately 58% of stations that exhibited decreasing trends. It was found that the magnitude of these trends was greater in the northern and southern areas of the YRD than they were in its central areas. Nevertheless, these findings were only significant in a minority of cases which were found to be distributed sporadically throughout the study region (Fig. 5g). These results are still in general agreement with past studies on the subject though (Fu et al. 2013). By contrast, only 33% of stations exhibited increasing trends, and none of them were found to be significant. Additionally, it is worth to noting that CDD displayed downtrends trends over the entire study region, and about 34% of them were found to be significant. The stations that observed the latter were concentrated in the north-western, south-western, and eastern areas of the YRD. As can be seen

in Fig. 5h, the stations situated in northern AHP and southern JSP demonstrated the largest of these changes. For SDII, about 91% of stations exhibited an increasing trend, and the magnitude of this increase was considerably larger in the study region's eastern and south-eastern areas than elsewhere. This was especially apparent in southern JSP, central AHP, the coastal regions of the YRD, and western ZJP. The significant declining trends were found to be spread sporadically around the northern reaches of AHP and JSP (Fig. 5i).

Overall, the increasing and decreasing trends in precipitation extremes revealed a dramatic spatial heterogeneity over the region. The significant trends in positive variation were located primarily along the study region's coastal plains. This demonstrates that coastal regions of the YRD are generally more sensitive to changes in climate and are at a higher risk of increased flooding than the region's inland areas.

3.4 Future variation trend of precipitation extremes

In order to explore the changes that are likely to occur in the trends for extreme precipitation in the future, the Hurst exponent was calculated using a rescaled range analysis. Generally speaking, the Hurst exponent for all extreme precipitation indices was found to be greater than 0.5, on average. The spatial distribution patterns were found to be like those for the study's historical sample period, namely from 1960 to 2016. A high level of sustainability for trends in the variation of extreme precipitation was found to be most likely in the YRD going into the future (Fig. 7). Looking at the study's indices individually, the highest value for the Hurst exponent was found in the result for SDII, while the lowest value was found in the result for R10 mm. In terms of specific stations, it can be seen

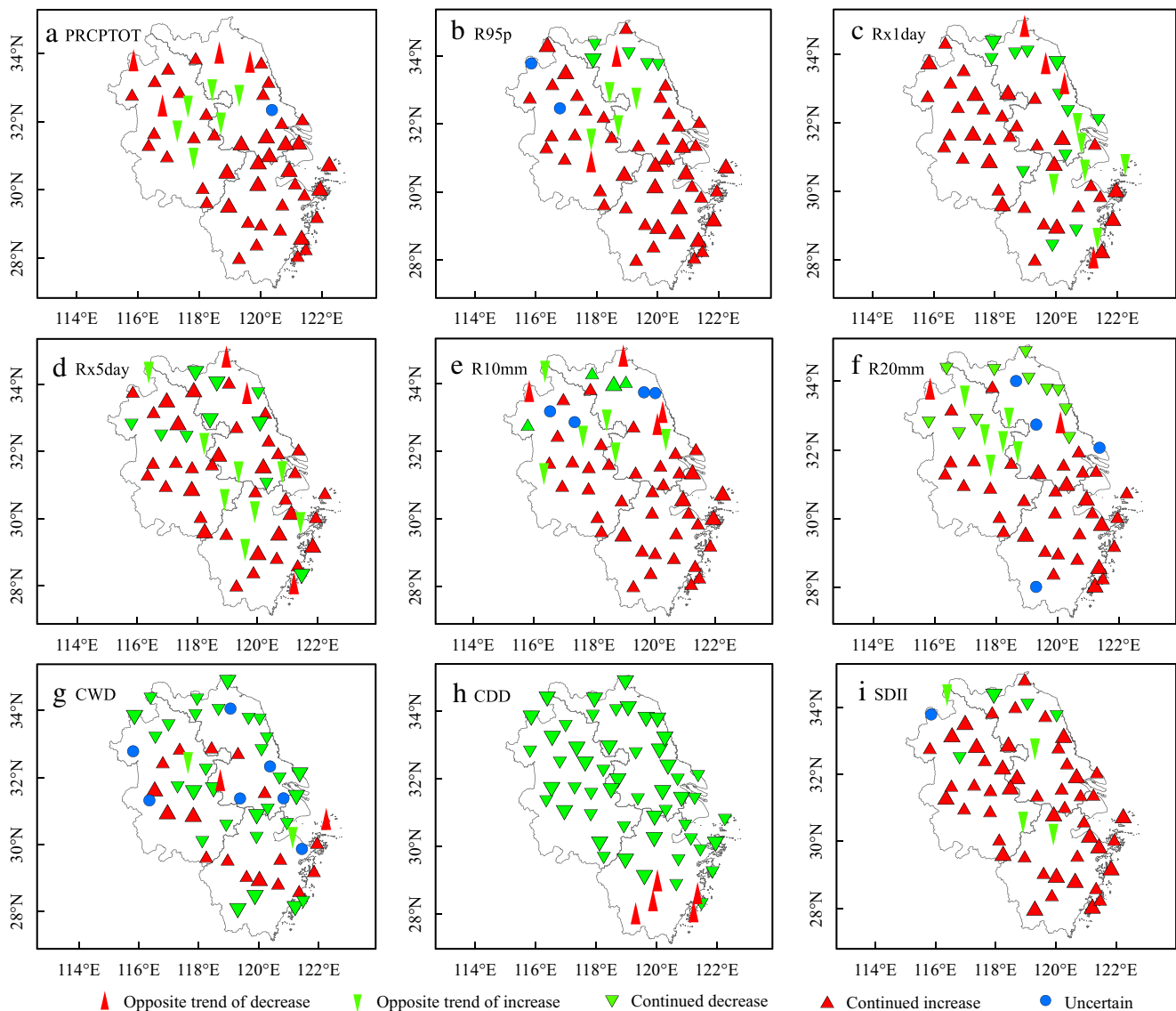


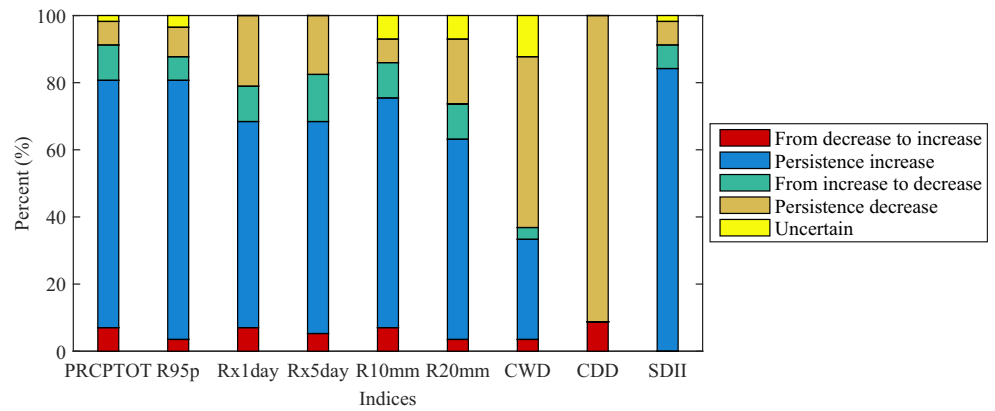
Fig. 7 Future variation patterns for the study's extreme precipitation indices from 1960 to 2016, for **a** PRCPTOT, **b** R95p, **c** Rx1day, **d** Rx5day, **e** R10 mm, **f** R20 mm, **g** CWD, **h** CDD, and **i** SDII. Red

denotes increasing trends or opposite trends of increase, blue denotes an uncertain trend, while green denotes decreasing trends or opposite trends of decrease

in Fig. 8 that the most obvious trends in sustained extreme precipitation were observed in SDII and CDD, with 84.21% of stations exhibited a sustained increasing trend and 91.23% of stations exhibited a sustained decreasing trend, respectively. In terms of the specific areas affected, eastern JSP, southeastern ZJP, and the central-north area of AHP exhibited a considerable increase in SDII, whereas the decreasing trend are located primarily in the northern area of the study region. Furthermore, for R95p, R10 mm, and R20 mm, it was found that the stations located in the central area of the YRD's eastern coast exhibited stronger increasing trends than for the region's western and southern areas.

Additionally, the most evident unsustainable trend can be seen for CDD and Rx5day in Fig. 8, with 8.8% of stations exhibiting a move from decrease to increase, and 14% of stations exhibiting a move from increase to decrease, respectively. The unsustainable trend for CDD was found to be concentrated in southern ZJP, whereas the unsustainable trend for Rx5day was generally distributed sporadically around southern JSP and AHP, just north of ZJP (Fig. 7d, h). It worth is noting that the stations that exhibited uncertain trends were located primarily in JSP and AHP, indicating that the changes in extreme precipitation for these regions are more complex than those for ZHP.

Fig. 8 The statistic for different types of future change across the YRD for each of the study’s indices



Overall, it is reasonable to speculate that the YRD will face a flood risk of increasing severity in the foreseeable future. This can be concluded when considering that the amounts, frequency, as well as intensity of extreme precipitation in the regions were all found to exhibit trends toward increase in this study’s inferential analyses. Regionally, the southern and central-western areas of the YRD will likely become wetter, which will generate greater pressure on local flood control infrastructure. Conversely, the regions located in the north of the YRD will likely become drier, which may well exacerbate local water supply problems.

4 Discussion

It is known that changes in precipitation extremes will be influenced by multiple factors. Example therein includes global warming, atmospheric circulation, urbanization, deforestation, the distance to coastline, and topography (IPCC 2013; Wang et al. 2014; Xu et al. 2018). A study conducted by Min et al. (2011) found that heavy precipitation events intensified in approximately two-thirds of their study’s observation stations, all located throughout the Northern Hemisphere, over the latter half of the twentieth century. In that study, it was concluded that this intensification was attributable to the human activities that induce increases in global greenhouse gases. The changes in the physical properties of land surface as a result of urbanization generate a considerable effect on local heat and water vapor. Therefore, a regional climate will be affected in many adverse ways in turn from such urbanization processes. Wang et al. (2014) indicated that, generally, urbanization works to induce an increasing rate of heavy precipitation events, and that urbanization in the Pearl River Delta region specifically has brought about diminished rates of light precipitation. However, the physical mechanisms behind how these factors impact changes in precipitation extremes are very complicated on more comprehensive scales (O’Gorman and Schneider 2009). To have a better understanding therein, more research is needed. Unfortunately, it

must point out here that this last goal is not within the scope of this study. Rather, this study focused primarily on the relationship between precipitation extremes and large-scale atmospheric circulation.

In this study, the PDO and MEI indices showed an insignificant and slightly upward trend from 1960 to 2016 (Fig. 9a, b). When compared with PDO, MEI indicated high rates of fluctuation, so that the duration of positive and negative phases was shorter. Before 1976, phases in PDO were primarily negative. Thereafter, PDO phases were primarily positive, up until 2006. Subsequently, an oscillation between negative and positive phases occurred, respectively, from 2007 to 2013 and from 2014 to 2016. Additionally, the study’s The EASMI revealed an insignificant downward trend. The intensity of this EASMI trend was found to exhibit strong interannual-to-decadal fluctuations. This was, especially the case in the final decade of the study period. As seen in Fig. 9c, the strength of the indices reaches its weakest point during the study period. It is likely that this situation was caused by a positive pressure anomaly originating from the regions around Northern China and Mongolia (Liu and Guo 2005).

The results of the study’s wavelet coherence analysis between large-scale atmospheric circulation and R95p are presented in Fig. 10. The thick black contours depict the 0.05 confidence level relative to red noise, while the black line denotes the cone of influence where edge effects may end up distorting results. The relative phase relationship is represented by the direction of the figure’s arrows. An in-phase correlation points to the right, while an anti-phase correlation points to the left (Grinsted et al. 2004; Zhang et al. 2007). The R95p index indicates that there is a statistically significant positive correlation between PDO and MEI during 1980s at scale of 2–4 years as well as 2–5 years, respectively (Fig. 10a, b). This implies that rainfall in the YRD became more plentiful when PDO and MEI were in a positive phase and vice versa. These findings are consistent with the results of Zhang et al. (2007), who reported that the annual maximum streamflow in the lower Yangtze Basin is in-phase with ENSO

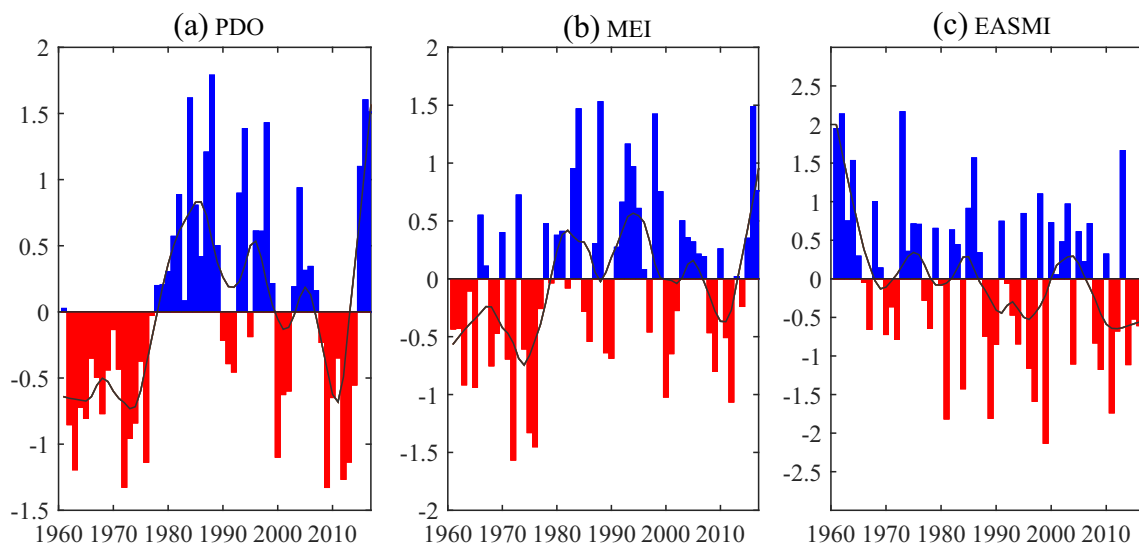


Fig. 9 The trend of the averaged anomaly series over time for **a** POD, **b** MEI, and **c** E ASMI. The thick black curves were obtained by using locally weighted smoothing (Cleveland and Devlin 1988)

events. In addition, more regions exhibited an insignificant positive correlation with MEI than with PDO, and it was found that the coefficients between MEI and R95p were larger than those between PDO and R95p. Thus, it can be concluded that the ENSO has more significant influence on R95p than PDO.

The study’s wavelet coherence analysis conducted between R95p and EASMI showed a significant negative correlation from 1980 to 1985 at 2–5-year intervals (Fig. 10c). This indicates that a weak EASMI possibly contributes to the increasing R95 observed in recent decades. This finding is in line with past researches conducted by Li and Zeng (2002,

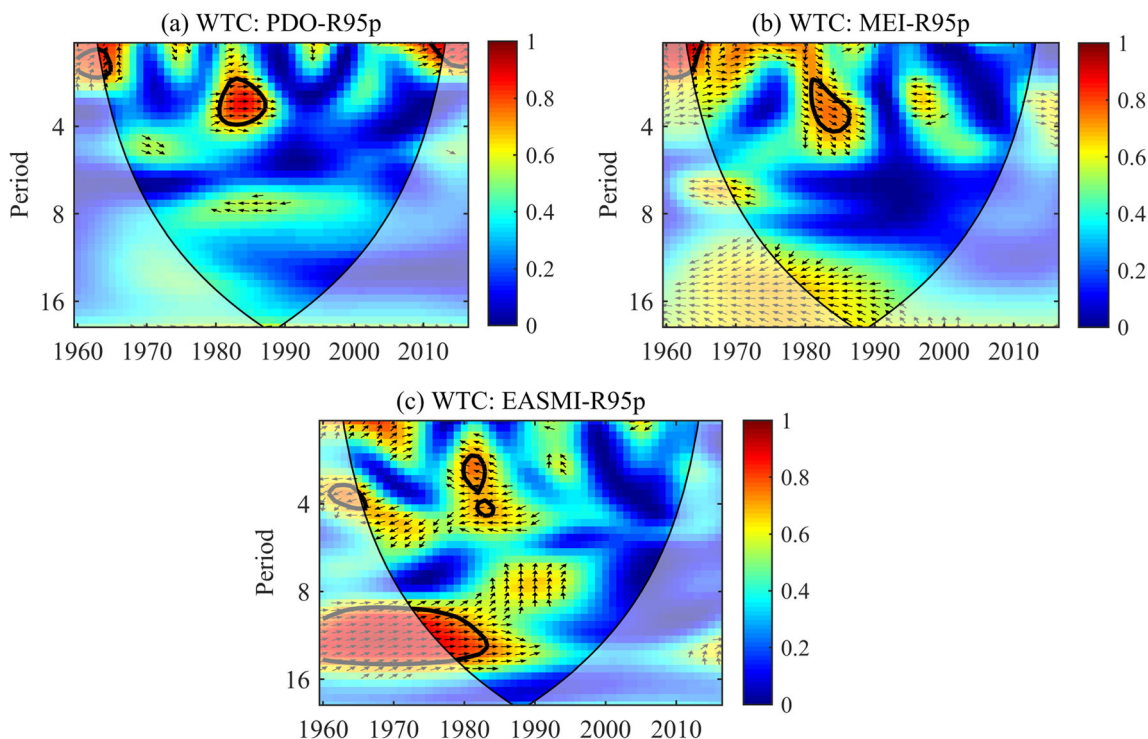


Fig. 10 The wavelet coherence found between **a** PDO and R95p, **b** MEI and R95p, and **c** EASMI and R95p. Red denotes high spectral power, which indicates periods characterized by high levels of extreme precipitation variance. Dark blue denotes low spectral power, which indicates periods characterized by low levels of extreme precipitation

variance. The thick black contours denote findings at the 5% confidence level of local power against red noise. The black line denotes the cone of influence. The right-pointing arrows indicate when the two signals will be in phase, while the left-pointing arrows denote antiphase signals

2005), who demonstrated that drought years and flood years over the middle and lower reaches of the Yangtze River are related to the annual intensity of the East Asian summer monsoon (EASM), respectively. On the other hand, some scientist's other researcher has further pointed out that, due to the weakening EASM intensity observed in recent years, the northward extension of the summer monsoon to northern China was limited, resulting in a southward movement of the region's major rain belts (Zhang et al. 2008). Consequently, the East Asian rainy season has become longer in the Yangtze River basin, and the number of the region's extreme precipitation events that occur in summer has subsequently increased, especially in the geographic middle and lower reaches of the Yangtze River (Wang and Zhou 2005; Liu and Guo 2005). Similar situations have also been observed in Korea as well as Japan (Li et al. 2010). More recently, Chen et al. (2018) simulated the changes that occur in monsoon-related rainfall generally, and the EASM specifically, under experiments that measured the effects that 1.5 °C and 2.0 °C warming will have over the twenty-first century. It was demonstrated that the location of EASM rain belt would not change significantly under such conditions, but that monsoon-related rainfall increases over most parts of East Asia under different warming scenarios.

Overall, these findings suggest that the changes in magnitude for extreme precipitation events in the YRD are linked to the observations found for MEI and EASMI. Moreover, the correlations found between PDO and R95p in the YRD from 1960 to 2016 are relatively weak compared with those of MEI.

5 Conclusions

In this study, the variability of precipitation extremes and their climatic teleconnection with large-scale atmospheric circulations were analyzed over the China's YRD from 1960 to 2016. The study's primary conclusions can be summarized as follows:

- (1) Seven of the study's nine extreme precipitation indices were generally dominated by positive trends. Significant increasing trends were found in the PRCPTOT, R95p, R10mm, R20mm, and SDII indices, indicating that the YRD became wetter overall during the study period. On the other hand, negative trends were observed in the CWD and CWDD indices, but none of them were found to be statistically significant. Furthermore, the contribution of R95p to PRCPTOT was found to increase significantly.
- (2) The patterns of distribution for precipitation extremes exhibited noticeable spatial heterogeneity. It was found that the indices' significant positive trend was located predominantly along the region's coastal plains. Thus,

these regions are at the highest risk of increased flooding. Additionally, calculating the Hurst exponent revealed that all extreme precipitation indices exhibited consistently high rates of variation in their extreme precipitation trends going into the foreseeable future. Thus, it can be also be concluded that the YRD will likely face increasingly severe flooding risk moving forward. Through the study's inferential analyses, it was found that the southern and central-western areas of the YRD will likely become wetter in the foreseeable future and that pressure on regional flood control infrastructure will increase over time, more so than with the YRD's other areas. Conversely, the northern areas of the YRD will likely become drier, and as such local problems of regarding water supply will likely be exacerbated.

- (3) Findings for the study's R95p index indicated that rainfall in the YRD will increase when PDO and MEI in their positive phase. A weak EASMI therein potentially contributes to the increasing trend found in recent decades for R95p. The trend toward increasing rates of precipitation extremes in the YRD was found to be closely linked to the positive anomalies of the ENSO and correspondingly linked with the negative anomalies of the EASM.

The variability of precipitation extremes that were observed over the study period will have important consequences for water resource management authorities operating in the YRD. Nevertheless, obtaining accurate precipitation data is not only a prerequisite for exploring the mechanisms behind changes in precipitation extremes, but also critical for developing effective water resource management strategies. Thus, it is important to evaluate and optimize existing gauges so they are better able to measure the extreme rainfall processes that occur in short periods of time. Furthermore, it is important to combine multiple data sources as well as model simulation results in studies on specific regions that face a high risk of future flooding in order to develop regional flood risk maps under various return periods, to better guide urban development, and to set strict but fair limits on land use as well as urban development in identified high-risk areas. Additionally, it is also crucial that improvements be made in real-time forecasting as well as floods warning capabilities with increased investments in innovative radar and microwave technology. In addition, it will be necessary to dredge and widen the main flood channel in the YRD to increase the region's flooding capacity. Furthermore, low impact development strategies can implement in both urban and wetland areas to increase vegetation coverage as well as to prolong rainfall concentration time and reduce peak flow. Moreover, the impact of climate change as well as human activity on the water cycles and flooding processes should also be considered in a more comprehensive fashion. Non-stationarity extreme value analysis can be used to assess possible deficiencies in

the existing hydraulic structures built for flood regulation in order to guide future engineering designs in changing environments.

For the regions where precipitation extremes exhibited a decline, however, it is critical to local authorities better develop the region's capacity to store water, distribute water, and conserve water, in order to ensure water accessibility for sustained living standards as well as agriculture output. Measures include rainfall harvesting and water pollution prevention can be implemented to increasing water availability to these ends. However, it must be acknowledged that water resource management is a complex process that involves the close coordination in engineering, environmental science, public health, and sociological fields (Fletcher et al. 2013). More effort is needed in both work as well as research to ensure the safety of the people living in China's YRD.

Acknowledgements We are gratefully acknowledging the National Meteorological Information Center, China Meteorological Administration for offering the meteorological data. The authors would like to express our cordial gratitude to the editors and anonymous reviewers for their professional and pertinent comments and suggestions which are greatly helpful for quality improvement of this manuscript.

Funding information This study was financially supported by the National Key Research and Development Program of China (No. 2016YFC0401502), the National Natural Science Foundation of China (No. 41771032), and Water Conservancy Science and Technology Foundation of Jiangsu Province (No. 2015003).

References

- Alexander LV, Zhang X, Peterson TC, Caesar J, Gleason B, Klein Tank AMG, Haylock M, Collins D, Trewin B, Rahimzadeh F, Tagipou A, Rupa Kumar K, Revadeka J, Griffiths G, Vincent L, Stephenson DB, Burn J, Aguilar E, Brunet M, Taylor M, New M, Zhai P, Rusticucci M, Vazquez-Aguirre JL (2006) Global observed changes in daily climate extremes of temperature and precipitation. *J Geophys Res* 111:D05109
- Asadieh B, Krakauer NY (2015) Global trends in extreme precipitation: climate models versus observations. *Hydrol Earth Syst Sci* 19(2): 877–891
- Bourrel L, Rau P, Dewitte B, Labat D, Lavado W, Coutaud A, Vera A, Alvarado A, Ordoñez J (2015) Low-frequency modulation and trend of the relationship between ENSO and precipitation along the northern to Centre Peruvian Pacific coast. *Hydrol Process* 29(6):1252–1266
- Chen L, Qu X, Huang G, Gong YF (2018) Projections of east Asian summer monsoon under 1.5 °C and 2 °C warming goals. *Theor Appl Climatol*. <https://doi.org/10.1007/s00704-018-2720-1>
- China Statistical Publishing (2017) National Bureau of statistics of the People's Republic of China. *China Statistical Yearbook*. (in Chinese)
- Cleveland WS, Devlin SJ (1988) Locally weighted regression: an approach to regression analysis by local fitting. *J Am Stat Assoc* 83: 596–610
- Curriero FC, Patz JA, Rose JB, Lele S (2001) The association between extreme precipitation and waterborne disease outbreaks in the United States, 1948–1994. *Am J Public Health* 91(8):1194–1199
- Curtis S (2008) The Atlantic multidecadal oscillation and extreme daily precipitation over the US and Mexico during the hurricane season. *Clim Dyn* 30(4):343–351
- Dietz EJ, Killeen TJ (1981) A nonparametric multivariate test for monotone trend with pharmaceutical applications. *J Am Stat Assoc* 76: 169–174
- Donat MG, Alexander LV, Yang H, Durre I, Vose R, Dunn RJH, Willett KM, Aguilar E, Brunet M, Caesar J, Hewitson B, Jack C, Klein TAMG, Kruger AC, Marengo J, Peterson TC, Renom M, Oría Rojas C, Rusticucci M, Salinger J, Elrayah AS, Sekele SS, Srivastava AK, Trewin B, Villarreal C, Vincent LA, Zhai P, Zhang X, Kitching S (2013) Updated analyses of temperature and precipitation extreme indices since the beginning of the twentieth century: the HadEX2 dataset. *J Geophys Res* 118:2098–2118
- Donat MG, Andrew LL, Alexander LV, O'Gorman PA, Maher N (2016) More extreme precipitation in the world's dry and wet regions. *Nat Clim Chang* 6:508–513
- Duan WL, He B, Takara K, Luo PP, Hu MC, Alias NE, Nover D (2015) Changes of precipitation amounts and extremes over Japan between 1901 and 2012 and their connection to climate indices. *Clim Dyn* 45:2273–2292
- Duhan D, Pandey A (2013) Statistical analysis of long term spatial and temporal trends of precipitation during 1901–2002 at Madhya Pradesh. *India Atmos Res* 122(3):136–149
- Fletcher TD, Andrieu H, Hamel P (2013) Understanding, management and modelling of urban hydrology and its consequences for receiving waters: a state of the art. *Adv Water Resour* 51:261–279
- Fu GB, Yu JJ, Yu XB, Ouyang RL, Zhang YC, Wang P, Liu WB, Min LL (2013) Temporal variation of extreme rainfall events in China, 1961–2009. *J Hydrol* 487:48–59
- Gan TY (1998) Hydroclimatic trends and possible climatic warming in the Canadian prairies. *Water Resour Res* 34:3009–3015
- Gao T, Wang HL (2017) Trends in precipitation extremes over the Yellow River basin in North China: changing properties and causes. *Hydrol Process* 31:2412–2428
- Grimm AM, Tedeschi RG (2009) ENSO and extreme rainfall events in South America. *J Clim* 22:1589–1609
- Grinsted A, Moore JC, Jevrejeva S (2004) Application of the cross wavelet transform and wavelet coherence to geophysical time series. *Nonlinear Process Geophys* 11:561–566
- Han LF, Xu YP, Yang L, Deng XJ (2015) Changing structure of precipitation evolution during 1957–2013 in Yangtze River Delta, China. *Stoch Env Res Risk A* 29(8):2201–2212
- Hirsch RM, Slack JR, Smith RA (1982) Techniques of trend analysis for monthly water quality data. *Water Resour Res* 18:107–121
- Hossain F, Jeyachandran I, Sr RP (2010) Dam safety effects due to human alteration of extreme precipitation. *Water Resour Res* 46:W03301
- Hurst H (1951) Long term storage capacity of reservoirs. *Trans Am Soc Civ Eng* 6:770–799
- IPCC (2013) *Climate change 2013: the physical science basis. Contribution of Working Group I to the fifth assessment report of the Intergovernmental Panel on Climate Change*. Cambridge University Press, Cambridge
- Kao SC, Ganguly AR (2011) Intensity, duration, and frequency of precipitation extremes under 21st-century warming scenarios. *J Geophys Res* 116:D16119
- Kendall MG (1955) *Rank correlation methods*. Charles Griffin, London
- Klein Tank AMG, Zwiers FW, Zhang X (2009) Guidelines on analysis of extremes in a changing climate in support of informed decisions for adaptation. WCDMP-72, WMO-TD/no.1500; 56 pp
- Kug JS, Jin FF, An SI (2009) Two types of El Niño events: cold tongue El Niño and warm pool El Niño. *J Clim* 22(6):1499–1515
- Li JP, Zeng QC (2002) A unified monsoon index. *Geophys Res Lett* 29(8): 1274

- Li JP, Zeng QC (2005) A new monsoon index, its interannual variability and relation with monsoon precipitation. *Clim Environ Res* 10:351–365
- Li JP, Wu ZW, Jiang ZH, He JH (2010) Can global warming strengthen the east Asian summer monsoon? *J. Clim* 23(24):6696–6705
- Limsakul A, Singhruck P (2016) Long-term trends and variability of total and extreme precipitation in Thailand. *Atmos Res* 169:301–317
- Liu YX, Guo YF (2005) Impact of pressure system anomaly over mid-high latitude on the interdecadal change of east Asian summer monsoon. *Plateau Meteor* 24:129–135
- Liu T, Li JP, Li YJ, Zhao S, Zheng F, Zheng JY, Yao ZX (2017) Influence of the may southern annular mode on the South China Sea summer monsoon. *Clim Dyn* 2017(s1):1–13
- Llabrés-Brustenga A, Rius A, Rodríguez-Solà R, Casas-Castillo MC, Redaño A (2019) Quality control process of the daily rainfall series available in Catalonia from 1855 to the present. *Theor Appl Climatol*. <https://doi.org/10.1007/s00704-019-02772-5>
- Mandelbrot BB, Wallis JR (1969) Robustness of the rescaled range R/S in the measurement of noncyclic long-run statistical dependence. *Water Resour Res* 5:967–988
- Min SK, Zhang X, Zwiers FW, Hegerl GC (2011) Human contribution to more-intense precipitation extremes. *Nature* 470:378–381
- O’Gorman PA, Schneider T (2009) The physical basis for increases in precipitation extremes in simulations of 21st-century climate change. *Proc Natl Acad Sci* 106:14773–14777
- Peterson TC, Manton MJ (2008) Monitoring changes in climate extremes: a tale of international collaboration. *Bull Am Meteorol Soc* 89:1266–1271
- Qin PH, Xie ZH (2016) Detecting changes in future precipitation extremes over eight river basins in China using RegCM4 downscaling. *J Geophys Res* 121:6802–6821
- Rau P, Bourrel L, Labat D, Melo P, Dewitte B, Frappart F, Lavado W, Felipe O (2017) Regionalization of rainfall over the Peruvian Pacific slope and coast. *Int J Climatol* 37(1):143–158
- Sánchez Granero MA, Trinidad Segovia JE, García Pérez J (2008) Some comments on Hurst exponent and the long memory processes on capital markets. *Phys A* 387:5543–5551
- Shimizu MH, Ambrizzi T, Liebmann B (2017) Extreme precipitation events and their relationship with ENSO and MJO phases over northern South America. *Int J Climatol* 37:2977–2989
- Sun X, Renard B, Thyer M, Westra S, Lang M (2015) A global analysis of the asymmetric effect of ENSO on extreme precipitation. *J Hydrol* 530:51–65
- Tapiador FJ, Navarro A, Levizzani V, García-Ortega E, Huffman GJ, Kidd C, Kucera PA, Kummerow CD, Masunaga H, Petersen WA, Roca R, Sánchez JL, Tao WK, Turk FJ (2017) Global precipitation measurements for validating climate models. *Atmos Res* 197:1–20
- Tedeschi RG, Grimm AM, Cavalcanti IFA (2015) Influence of central and east ENSO on extreme events of precipitation in South America during austral spring and summer. *Int J Climatol* 35:2045–2064
- Torrence C, Compo GP (1998) A practical guide to wavelet analysis. *Bull Am Meteorol Soc* 79:61–78
- Wan L, Zhang XP, Ma Q, Zhang JJ, Ma TY, Sun YP (2014) Spatiotemporal characteristics of precipitation and extreme events on the loess plateau of China between 1957 and 2009. *Hydrol Process* 28:4971–4983
- Wang YQ, Zhou L (2005) Observed trends in extreme precipitation events in China during 1961–2001 and the associated changes in large-scale circulation. *Geophys Res Lett* 32:L09707
- Wang XM, Liao JB, Zhang J, Shen C, Chen WH, Xia BC, Wang TT (2014) A numeric study of regional climate change induced by urban expansion in the Pearl River Delta, China. *J. Appl Meteorol Clim* 53:346–362
- Wang YF, Xu YP, Lei CG, Li G, Han LF, Song S, Yang L, Deng XJ (2016) Spatio-temporal characteristics of precipitation and dryness/wetness in Yangtze River Delta, eastern China, during 1960–2012. *Atmos Res* 172–173:196–205
- Ward PJ, Jongman B, Kumm M, Dettinger MD, Weiland FCS, Winsemius HC (2014) Strong influence of El Niño southern oscillation on flood risk around the world. *Proc Natl Acad Sci* 111:15659–15664
- WMO (World Meteorological Organization) (2009) Guidelines on Analysis of Extremes in a Changing Climate in Support of Informed Decisions for Adaptation, Clim. Data and Monitoring, WCDMP-No. 72, Geneva
- Xiao MZ, Zhang Q, Singh VP (2017) Spatiotemporal variations of extreme precipitation regimes during 1961–2010 and possible teleconnections with climate indices across China. *Int J Climatol* 37:468–479
- Xu M, Kang SC, Wu H, Yuan X (2018) Detection of spatio-temporal variability of air temperature and precipitation based on long-term meteorological station observations over Tianshan Mountains, Central Asia. *Atmos Res* 203:141–163
- Yin YX, Xu CY, Chen HS, Li L, Xu HL, Li H, Jain SK (2016) Trend and concentration characteristics of precipitation and related climatic teleconnections from 1982 to 2010 in the Beas River basin, India. *Glob Planet Chang* 145:116–129
- Zhang Q, Xu CY, Jiang T, Wu YJ (2007) Possible influence of ENSO on annual maximum streamflow of the Yangtze River, China. *J Hydrol* 333(2):265–274
- Zhang Q, Xu CY, Zhang ZX, Chen YQD, Liu CL, Lin H (2008) Spatial and temporal variability of precipitation maxima during 1960–2005 in the Yangtze River basin and possible association with large-scale circulation. *J Hydrol* 353(3–4):215–227
- Zhang Q, Singh VP, Li JF, Chen XH (2011a) Analysis of the periods of maximum consecutive wet days in China. *J Geophys Res* 116:D23106
- Zhang XB, Alexander L, Hegerl GC, Jones P, Tank AK, Peterson TC, Trewin B, Zwiers FW (2011b) Indices for monitoring changes in extremes based on daily temperature and precipitation data. *WIREs Clim Change* 2(6):851–870
- Zhang Q, Peng JT, Xu CY, Singh VP (2014) Spatiotemporal variations of precipitation regimes across Yangtze River basin, China. *Theor Appl Climatol* 115(3/4):703–712